

Cite this: *J. Mater. Chem. A*, 2019, 7, 24776Received 20th August 2019
Accepted 15th October 2019

DOI: 10.1039/c9ta09125d

rsc.li/materials-a

In search of the most active MN4 catalyst for the oxygen reduction reaction. The case of perfluorinated Fe phthalocyanine†

Gabriel Abarca,^a Marco Viera,^b Carolina Aliaga,^{bc} José F. Marco,^d Walter Orellana,^e José H. Zagal^{*b} and Federico Tasca^{id}^{*b}

Iron macrocyclic complexes (MN4) are promising catalysts for replacing platinum (the industrial standard) in electrocatalysis. In particular, FeN4 complexes have shown lower overpotential than Pt for the oxygen reduction reaction (ORR) in alkaline media. To predict the electrochemical activity of metal electrodes and molecular catalysts towards the ORR, reactivity descriptors with typical volcano correlation have been demonstrated. The most important are M–O₂ binding energy and M⁽ⁿ⁾⁺/M⁽ⁿ⁻¹⁾⁺ redox potentials for the complexes. We studied a new Fe complex, which possesses powerful electron-withdrawing fluorine residues at the periphery of the phthalocyanine ring. Fe hexadecafluorophthalocyanine (16(F)FePc) was characterized by electron paramagnetic resonance (EPR), and X-ray photoelectron spectroscopy (XPS) in the presence and in absence of O₂. Experimental and calculated O₂–Fe binding energies, as well as electrochemical characterization confirms the excellent activity of this complex for the ORR placing this complex at the top of the MN4 volcano correlation.

1. Introduction

Metal macrocyclic complexes (MN4) are extremely versatile compounds that act as catalysts for a wide variety of electrochemical reactions.^{1–3} However they have been investigated extensively in the literature as potential catalysts for the oxygen reduction reaction (ORR) since 1964.⁴ The goal of these studies has been to develop substitutes for expensive Pt-containing catalysts for the O₂ cathode in fuel cells.⁵ In spite of these

efforts MN4 catalysts can compete with Pt in activity and stability only in alkaline media,⁶ whereas there are few of this class of catalyst that can compete in acidic conditions.⁵ Activity and stability seems to be correlated.⁷ Indeed when increasing the activity of the catalyst lower amounts of H₂O₂ are produced⁸ and therefore stability also increases. The activity of MN4 complexes can be improved by heat-treatment or by preparing catalysts with high Fe(II)/Fe(III) redox potential.^{9–14} It is imperative therefore to develop reactivity descriptors for these catalysts in order to rationally prepare materials.^{1,8,9,12,15,16} In previous work, the kinetic data of OPG electrodes modified with a great variety of substituted and non-substituted phthalocyanines and porphyrins of different central metals has been reported in order to establish reactivity descriptors for these catalysts for the ORR.^{11,17–19} Several reactivity descriptors have been identified but the most important ones are the M–O₂ binding energy and the M⁽ⁿ⁾⁺/M⁽ⁿ⁻¹⁾⁺ redox potentials of the complexes.^{11,16} It has been shown that these two descriptors linearly correlate with each other.¹⁶ When comparing activities of different molecular catalysts (log *i*)_E at the constant driving force of the electrode *versus* the M–O₂ binding energy of each particular catalyst a non-linear, volcano-shaped curve is obtained. These types of correlations are well-known for metals, alloys and metal oxides but less common for molecular catalysts.^{16,20} There is a similarity in the trend in reactivity for molecular catalysts and for metal catalysts. A similar correlation is obtained when comparing log of activities as (log *i*)_E *versus* the M⁽ⁿ⁾⁺/M⁽ⁿ⁻¹⁾⁺ redox potential of the catalysts. Volcano correlations depict two binding energy conditions: one leg of the volcano, with a positive slope corresponding to the strong binding catalysts and the other volcano leg corresponding to the weak binding region.¹⁶ According to the literature, all FeN4s appear on the strong binding leg of the volcano and catalyze ORR *via* 4 electrons involving the splitting of the O–O bond.¹⁶ On the other leg of the volcano are the catalysts that catalyze ORR *via* 2 electrons like Co and Ni complexes. According to linear scale relationships strong O₂ binding will correlate linearly with strong peroxide binding so this could explain the 4 e[–] selectivity of catalysts

^aCentro de Nanotecnología Aplicada, Facultad de Ciencias, Universidad Mayor, Santiago, Chile

^bFacultad de Química y Biología, Universidad de Santiago de Chile, Santiago, Chile. E-mail: jose.zagal@usach.cl; federico.tasca@usach.cl

^cCenter for the Development of Nanoscience and Nanotechnology, CEDENNA, Santiago, Chile

^dInstituto de Química Física “Rocasolano”, CSIC, Madrid, Spain

^eDepartamento de Ciencias Físicas, Universidad Andres Bello, Sazié 2212, 837-0136 Santiago, Chile

† Electronic supplementary information (ESI) available. See DOI: 10.1039/c9ta09125d

sitting on the strong binding leg of a volcano correlation.^{16,21} In this case the peroxide intermediate that can form during ORR remains bound to the active site, facilitating its further reduction to H₂O or OH⁻. In this work we have investigated a new catalyst for ORR, iron-hexadecafluorophthalocyanine (16(F)FePc) that has powerful electron-withdrawing F residues that hypothetically should have the highest activity among all the MN₄ complexes and therefore would be sited at the top of the volcano correlation. The complex was characterized by EPR and XPS spectroscopy in the presence and absence of O₂. Experimental O₂-Fe binding energies and calculated ones, as well as electrochemical characterization confirm the highest activity of this complex towards the ORR.

2. Experimental

Iron 1,2,3,4,8,9,10,11,15,16,17,18,22,23,24,25-hexadeca(fluoro)phthalocyanine (16(F)FePc) was obtained from Luminescence Technology Corp (New Taipei City, Taiwan) and used as provided. *N,N*-dimethylformamide (DMF), isopropyl alcohol, NaOH, H₂SO₄, K₂HPO₄ were obtained from Sigma (St. Louis, USA). Pt catalyst, 20% Pt supported on Vulcan XC-72 carbon (Pt20%Vulcan), was from Fuel Cell Store (College Station, Texas). Aqueous solutions were prepared using Milli Q water (Millipore, Inc.). Double-walled CNT were obtained from Nanocyl (Sambreville, Belgium). Double-walled CNT were used instead of multi- or single-walled CNT because of their higher purity (>90%).^{22,23} CNT were used as support because of their high surface to volume ratio and the possibility to support higher amounts of catalyst.¹⁷ To modify electrodes an ink of 16(F)FePc-CNT was obtained by dispersing 1 mg of 16(F)FePc with 1 mg of CNT to obtain 16(F)FePc-CNT in a solution of 75% volume isopropyl alcohol and 25% water. The dispersion was sonicated for 1 h and collected by filtering and washing to eliminate excess of 16(F)FePc which would not adsorb on the CNT walls. An ink of Pt catalyst was obtained by dispersion and sonication of 1 mg of catalyst in 1 mL of similar solvent. 20 μL of catalyst ink were loaded onto the surface of the electrode and left to dry (final loading was 0.1 mg cm⁻²). The counter electrode was a 10 cm long 0.1 cm diameter Pt spiral wire. As reference electrode an Orignalys (Rillieux-la-Pape, France) 3 M KCl Hg|HgCl was used and all the potentials are reported vs. this electrode. The working electrode was an edge-plane pyrolytic rotating disk graphite (5 mm diameter and 4 mm thick), mounted in Teflon (external diameter of 7.50 mm, internal diameter of 6.50 mm) and was rotated using a MSR rotator from Pine Instruments (Durham, NC, USA). The graphite disk was renewed prior to modification with 800 grit emery paper. Electrochemical experiments were carried out on an Autolab PGSTAT 302N with a dual mode bipotentiostat module (Utrecht, The Netherlands). In RRDE experiments, the ring potential was set to 0.65 V vs. Hg|HgCl (saturated KCl). For EPR and XPS measurements a dried powder of MN₄-CNT was used. EPR spectra were collected at 298 K with a Bruker EMX-1572 spectrometer working at ~9.39 GHz (X-band). For the XPS measurements, the sample powder of 16(F)FePc-CNT was spread out on carbon tape and introduced into the analysis

chamber at the soft X-ray spectroscopy (SXS) beam-line end-station at the Brazilian Synchrotron Light Laboratory. As reported before,²⁴ room temperature O₂ treatment was conducted in the preparation chamber using a pressure of 20 psi of 5% O₂ + 95% He over two hours. The spectra were collected using an InSb (111) double-crystal monochromator at a fixed photon energy of 1840 eV. The hemispherical electron analyser (PHOIBOS HSA500 150 R6) was set at a pass energy of 30 eV, and the energy step was 0.1 eV. The base pressure used inside the chamber was around 2.0 × 10⁻⁹ mbar. The monochromator photon energy calibration was done at the Si K edge (1839 eV). An additional calibration of the analyser's energy was performed using standard Au foil (Au 4f_{7/2} peak at 84.0 eV). Curve fitting of the core XPS lines was carried out using Casa XPS software using a Gaussian-Lorentzian product function and a nonlinear Shirley background subtraction.

Spin-polarized density functional theory (DFT) calculations were performed with the Quantum-ESPRESSO *ab initio* package.²⁵ The dispersive (π-stacking) interaction of 16(F)FePc adsorbed on the carbon nanotube (CNT) was included through the van der Waals exchange-correlation functional (vdW-DF2).²⁶ Kohn-Sham eigen-functions were expanded on a plane-waves basis set where the interaction between valence electrons and ion cores are described by ultra-soft pseudo-potentials.²⁷ Converged results have been achieved by using cut-off energies of 35 Ry on plane waves and of 280 Ry on the electronic density. The 16(F)FePc-CNT complex was simulated in a large unit cell, containing up to 345 atoms, with periodic boundary conditions. A metallic single-walled CNT with (8,8) chiral indexes and 11 Å in diameter was considered. The sampling in the irreducible part of the Brillouin zone was restricted to the *Γ* point. The complex was fully relaxed until the force on each atomic component was less than 0.01 eV Å⁻¹. The ORR catalytic activity of 16(F)FePc-CNT complex was estimated by assessing the minimum energy path for the O₂ dissociation after being adsorbed on the Fe atom, using the nudged elastic band (NEB) method.²⁸

3. Results and discussion

In the volcano correlation reported previously (see graphical abstract with the exclusion of the apex), there were no catalysts sitting on the apex of the plot. Hypothetically, a catalyst could exist that has the proper M(III)/(II) redox potential or M-O₂ binding energy to stand at the top of the correlation, so essentially this could be the best possible catalyst for the reaction. In this work iron-hexadecafluorophthalocyanine, 16(F)FePc, adsorbed on carbon nanotubes (*i.e.* 16(F)FePc-CNT) was tested. The synthesis of 16(F)FePc was first reported in 1969 by Jones and Twigg,²⁹ but, to the best of our knowledge, the electrochemistry of this compound and its catalytic properties for the ORR have never been reported. This particular complex has more powerful electron-withdrawing substituents on the phthalocyanine ligand, so the Fe(III)/(II) is shifted to more positive potentials compared to all previously reported catalysts.^{1,13,16,17} Fig. 1 illustrates the configuration of a 16(F)FePc molecule adsorbed flat on the graphene layer of a CNT or

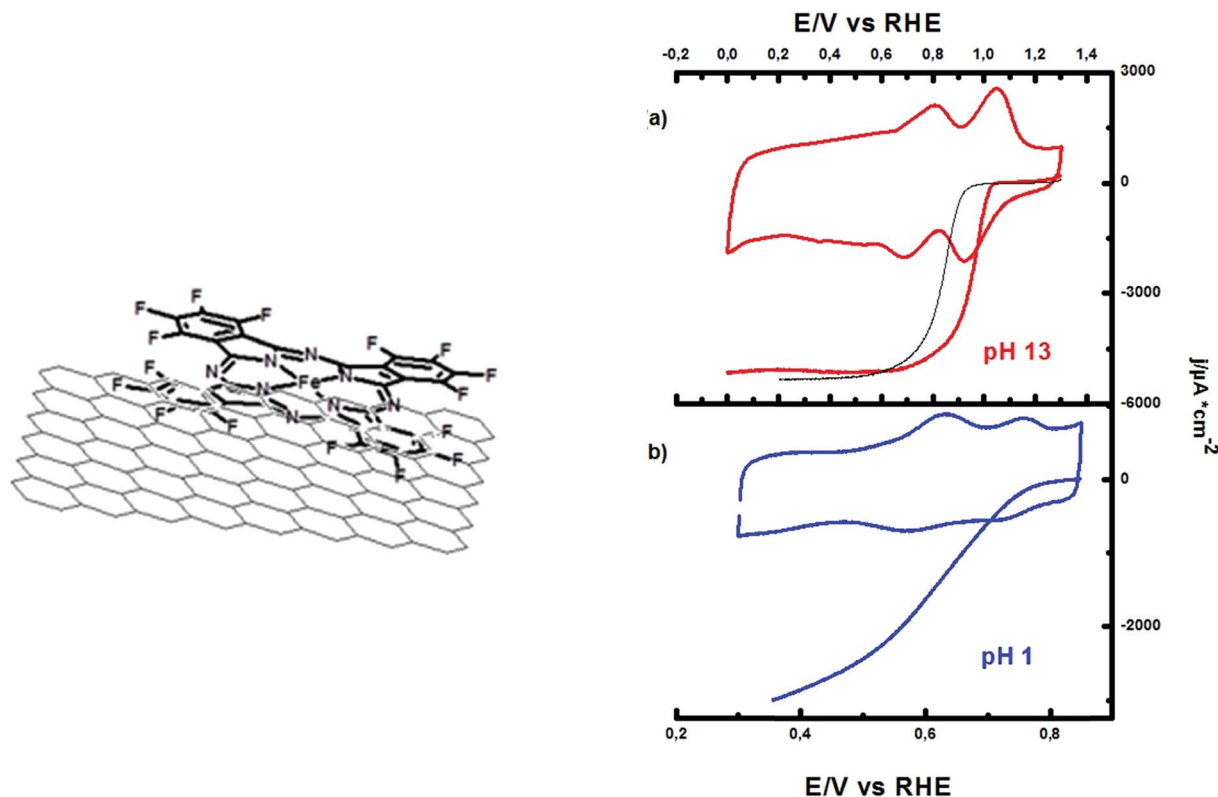


Fig. 1 Schematic representation of 16(F)FePc adsorbed on CNT and electrochemical characterization by cyclic voltammetry in N₂ saturated media and by linear sweep voltammetry in O₂ saturated media of electrodes modified with 16(F)FePc-CNT (blue and red lines) or Pt20%Vulcan (black line). Conditions (a) 0.1 M NaOH; (b) 0.1 M H₂SO₄. Cyclic voltammetry recorded at 100 mV s⁻¹; linear sweep voltammetry recorded at 5 mV s⁻¹, 1200 rpm.

a graphite electrode and typical cyclic voltammogram of graphite electrodes modified with 0.1 mg cm⁻² of 16(F)FePc-CNT, in N₂ saturated 0.1 M NaOH (Fig. 1(a)) or H₂SO₄ solutions (Fig. 1(b)). For comparison, we report the linear sweep voltammetry of electrodes modified with Pt20%Vulcan (black line), the industrial standard catalyst for the ORR. The Fe(III)/(II) redox peaks appear at potentials close to 1 and +0.75 V vs. RHE at pH 13 and 1 respectively. Table 1 reports these values as well as the values for the Fe(II)/(I) redox peak. Because of the strong electron-withdrawing F residues, which are distributed in all peripheral and non-peripheral positions in the phthalocyanine ligand 16(F)FePc exhibits the most positive redox potential for the Fe(III)/(II) couple among the previously studied FeN₄ (e.g. 0.9 V for iron hexadecachloro phthalocyanine 16(Cl)FePc¹⁷ and 0.95 V for Fe tetrapyrrolineporphyrazine, at pH 13 (ref. 30)). The

Fe(III)/(II) redox peak of MN₄ usually shows a 60 mV pH⁻¹ unit dependence in the wide range of pH 13–1 as the process involves the transfer of an OH⁻ ion as [Fe(III)OH]_{ad} + e ⇌ [Fe(II)]_{ad} + OH_(aq)⁻.³¹ MN₄ complexes were known to be unstable in acid during the ORR process. It is probable that demetallation of the metal site occurs because of the production of H₂O₂ as a result of the ORR in acid media. In a recent publication, the activity of penta-coordinated FePc catalyst at pH 1 was reported.³² The fifth pyridine axial coordination pulls electron density from the Fe centre, lowering the separation between the energies of the frontier orbitals of the donor (Fe) and the acceptor (O₂), resulting in increased activity towards the ORR. Following the idea that the activity of MN₄ can be increased also in acid media with the increasing electron-withdrawing power of the residues in the phthalocyanine macrocycle, the 16(F)

Table 1 Electrochemical parameters of 16(F)FePc-CNT. Redox potential of Fe(II)/(I) or Fe(III)/(II); number of electrons calculated from the Koutecky–Levich equation; Tafel slope; surface coverage (T); onset from the O₂ reduction polarization curves

Catalyst	Media	$E_{(M(I)/(II))}$ (V vs. RHE)	$E_{(M(II)/(III))}$ (V vs. RHE)	$n^{\circ} e^{-}$	Tafel (V)	T (mol × cm ⁻²)	ONSET (V vs. RHE)
16(F)FePc-CNT	0.1 M NaOH	0.750	0.99	4.05	-0.046	1.18×10^{-9}	1.055
16(F)FePc-CNT	0.1 M H ₂ SO ₄	0.610	0.75	3.45	-0.073	2.71×10^{-9}	0.810
Pt20%Vulcan	0.1 M NaOH	—	—	4.01	-0.047	4.50×10^{-10}	0.995
Pt20%Vulcan	0.1 M H ₂ SO ₄	—	—	4.01	-0.048	2.83×10^{-10}	0.955

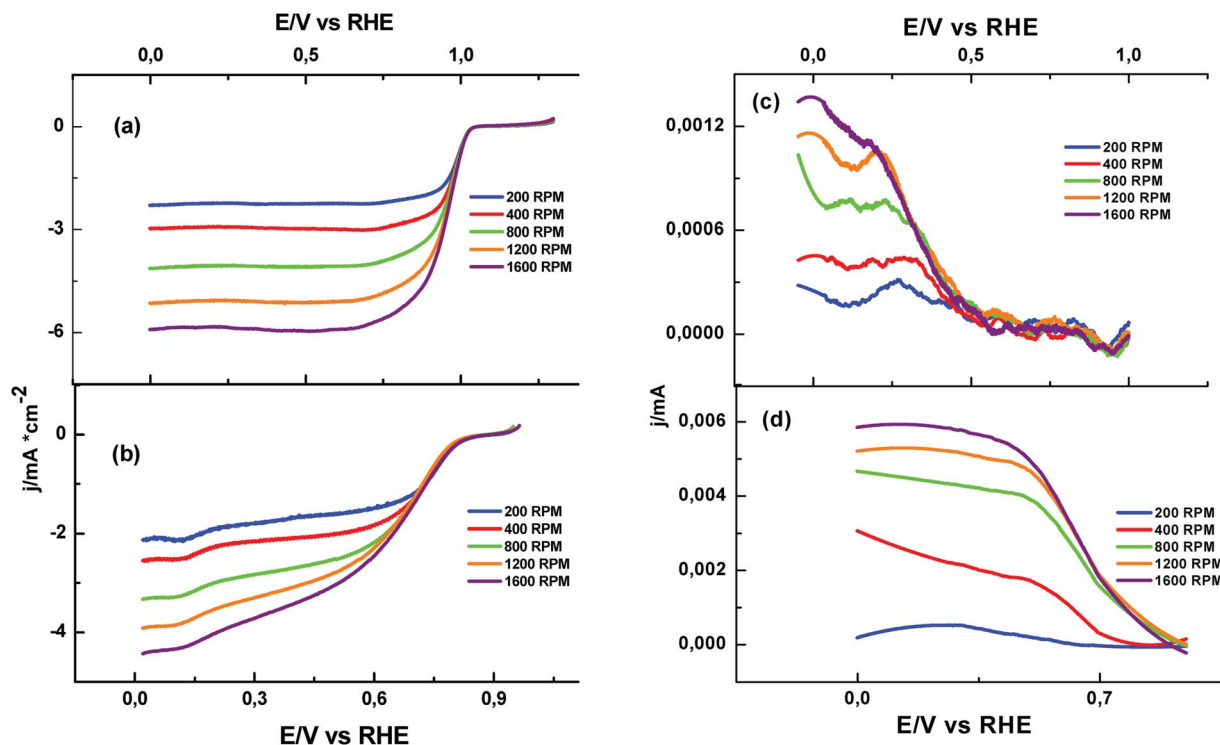


Fig. 2 Polarization curves and relative H_2O_2 oxidation curves recorded at electrodes modified with 16(F)FePc-CNT (disks) and Pt ring electrode. Conditions: (a and c) O_2 saturated 0.1 M NaOH solution. (b and d) O_2 saturated 0.1 M H_2SO_4 solution. Rotating ring disk electrode velocity: 200, 400, 800, 1200, and 1600 rpm, 5 mV s^{-1} ; Pt ring polarized at 1.3 V vs. RHE.

FePc-CNT was tested in acid. Fig. 2 illustrates the ORR polarization curves at various rotating speeds in O_2 saturated 0.1 M NaOH or H_2SO_4 solutions. Because of the high redox potential of the Fe(III)/II redox couple the onset for the ORR at pH 13 appears already at potentials above 1.05 V. The overpotential for the ORR is reduced by more than 0.16 V if compared to FePc-CNT and to almost 0.1 V if compared to 16(Cl)FePc-CNT measured in the same media.¹⁷ At pH 1 the onset for the ORR appears already at 0.81 V, that is to say a diminution of the overpotential for the ORR of around 0.1 V if compared to FePc-CNT and of 0.05 V if compared to 16(Cl)FePc-CNT in similar media.³² In Fig. 2(c) and (d) H_2O_2 oxidation current recollected at the Pt ring electrode during linear sweep voltammetry at pH 13 and at pH 1 are presented. At pH 1, five times more H_2O_2 was produced than at pH 13, demonstrating the higher activity of the 16(F)FePc at pH 13 and therefore the lower stability at pH 1. If we compare those results with the ones obtained with Pt20% Vulcan, we can notice that the onset for the ORR at pH 13 for 16(F)FePc occurs at 0.06 V lower overpotentials. Nevertheless it should be considered that the concentration of active Pt on the graphite electrode modified with Pt20%Vulcan is almost one order of magnitude lower than the amount of active Fe(III)/II in 16(F)FePc-CNT (see Table 1 for the resumed values).

The extrapolation of the total $n^\circ e^-$ determined by the Koutecky-Levich equation for pH 13 and pH 1 are summarized in Table 1. The alkaline pH favored $4 e^-$ reduction (4.0 electrons per O_2 molecule). Nevertheless, at pH 1, 3.45 electrons were transferred per O_2 molecule indicating a mixed reaction

pathway. From Tafel plots using currents in the low polarization linear region values $\approx -0.046 \text{ V}$ were obtained while at pH 1, the Tafel slopes were $\approx -0.073 \text{ V}$. Slopes close to -0.04 V indicated that the first step involved a fast one-electron transfer followed by a slow one-electron transfer while values close to -0.060 V suggested that the first step involves a fast electron transfer followed by a slow rate determining chemical step. The change in ET mechanism going from alkaline solution to acid solution has been observed before for similar FeN4 complexes.³³

Turn over frequencies (TOFs) were estimated for the 16(F)FePc-CNT modified electrode from the coverage of the electrode Γ and the kinetic current densities at the half wave potential of the ORR polarization curve, with values ranging from 5.4 s^{-1} to 3.4 s^{-1} for pH 13 and pH 1 respectively (values listed in Table 2). At pH 13, TOF values of 5.2 s^{-1} were calculated for electrodes modified with 16(Cl)FePc-CNT or the unsubstituted iron phthalocyanine (FePc-CNT).¹⁷ At pH 1, TOF values of 0.2 and 0.02 s^{-1} were calculated for 16(Cl)FePc-CNT and FePc-CNT respectively. Therefore, similar TOF values were obtained in alkaline media, but at pH 1, one order magnitude higher TOF values were obtained with the 16(F)FePc catalyst because of its lower electron density in the metal center and higher activity towards the ORR. If we compare the TOF values obtained for 16(F)FePc-CNT with the ones obtained for Pt%20Vulcan, we can notice that the 2 catalyst show similar TOF at low overpotential (*i.e.* at 0.9 V vs. RHE) in alkaline media, only because of the lower onset for the ORR of 16(F)FePc-CNT. If we compare the 2 catalyst close to the limiting current region (*i.e.* at

Table 2 TOF calculated at 0.9, 0.8, 0.7 V vs. RHE or at half wave potential. Conditions: O₂ saturated, 0.1 M NaOH or H₂SO₄ solutions

Catalyst	Media	TOF @ 0.9 V (s ⁻¹)	TOF @ 0.8 V (s ⁻¹)	TOF @ 0.7 V (s ⁻¹)	TOF @ hw (s ⁻¹)
16(F)FePc-CNT	0.1 M NaOH	0.99	6	11	5.4
16(F)FePc-CNT	0.1 M H ₂ SO ₄	—	—	2.8	3.4
Pt20%Vulcan	0.1 M NaOH	0.8	12.1	18.4	11.3

0.7 V vs. RHE), TOF numbers for Pt%20Vulcan are in the order of 18 s⁻¹ while for the 16(F)FePc-CNT catalyst values of 11 and 2.8 s⁻¹ were obtained at pH 13 and pH 1 respectively, as resumed in Table 2.

EPR and XPS spectroscopy confirmed that in 16(F)FePc-CNT the electrons are displaced from the Fe centre because of the pulling effect of F atoms.^{34,35} In Fig. 3(a) EPR spectra of 16(F)FePc-CNT and 16(F)FePc are reported. The strong electron-withdrawing effect of the F substituents on the electron environment on the odd spin of the metallic centre of the porphyrin shows a higher value of *g* (2.06909) if compared to the unsubstituted porphyrin (*i.e.* FePc-CNT) 2.06494 or to the perchlorinated FeN4 (*i.e.* 16(Cl)FePc-CNT) 2.06574.

XPS in the presence and the absence of O₂ coordinated to the Fe metal center was performed to verify the electronic structure of the 16(F)FePc-CNT. Distinct peaks in F 1s, Fe 2p, O 1s, N 1s and C 1s regions, confirmed the attachment of 16(F)FePc on the external surface of the CNT (Fig. S1†). The atomic composition of 16(F)FePc-CNT, between the Fe 2p peak and F 1s peak, was obtained within experimental error 1 : 16.8. The Fe 2p region was analyzed for providing further insights into the catalytic behavior of 16(F)FePc-CNT (Fig. 3(b) and S2†). Two broad spin-orbit doublet Fe 2p peaks indicated the presence of Fe in different valence states, with the main component being a mixture of Fe(II) and Fe(III).^{32,36,37} The binding energy of the Fe 2p_{3/2} photoelectron line of 16(F)FePc-CNT was located at 710.2 eV, and a satellite peak (shake-up) at 7.4 eV higher was also observed, which is easily detectable and does not overlap with Fe 2p peaks. These peaks were in good agreement with

reported binding energies and resembled the spectra of some phthalocyanines reported containing only Fe(III).³² It is important to note, that satellite peaks represent the intermolecular charge transfer process, where the intensity of these peaks can be related to the amount of charge transferred between the fragments of the macrocycle and the iron center.³⁸ This phenomenon can be correlated with the Franck–Condon effect, where it occurs after an electron is removed from the sample (photoemission) and the sample suffers an inner-sphere reorganization.^{39,40} After the exposition to O₂ (Fig. 3(b), red line), a significant energy shift of 1.5 eV was observed (708.7 eV for Fe 2p_{3/2}). According to previous work, this second contribution agrees with the presence of Fe(II).^{24,32} Moreover, after the exposure to O₂ an increased Fe(II)/Fe(III) ratio was observed (from 1.27 ratio when reduced to 1.38 ratio when oxidized, Fig. S2†). These results suggest the presence of a more stable Fe–O₂ adduct.^{24,32,41,42} It can be concluded that after the exposition to O₂, an increased character of Fe(II) exists due to the presence of electron-withdrawing groups, that can tune the electron density towards the molecular fragments. When O₂ binds to the metal in MN₄, its 2p electrons interact with the partially filled d orbitals of the same. These processes are accompanied by intermolecular electron transfer, in which O₂ accepts charge density from the partially filled d orbitals of the metal *via* back-bonding to the p* antibonding orbital and donates charge from a filled p molecular orbital to a half-filled d_z orbital of the metal.³²

Results from theoretical calculations show that 16(F)FePc-CNT complex can exist in three spin states, which is due to

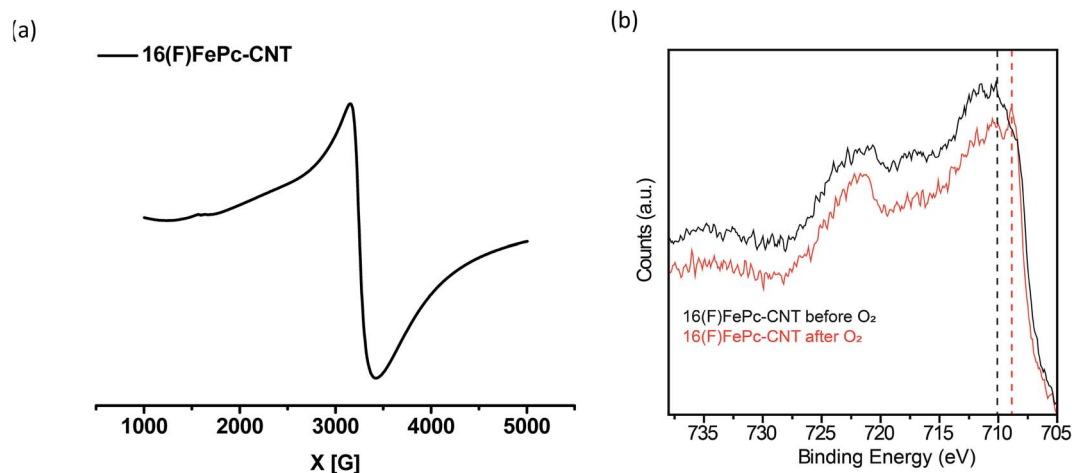


Fig. 3 (a) EPR spectrum of 16(F)FePc-CNT. (b) XPS spectrum of 16(F)FePc-CNT before (black line) and after (red line) treatment with O₂.

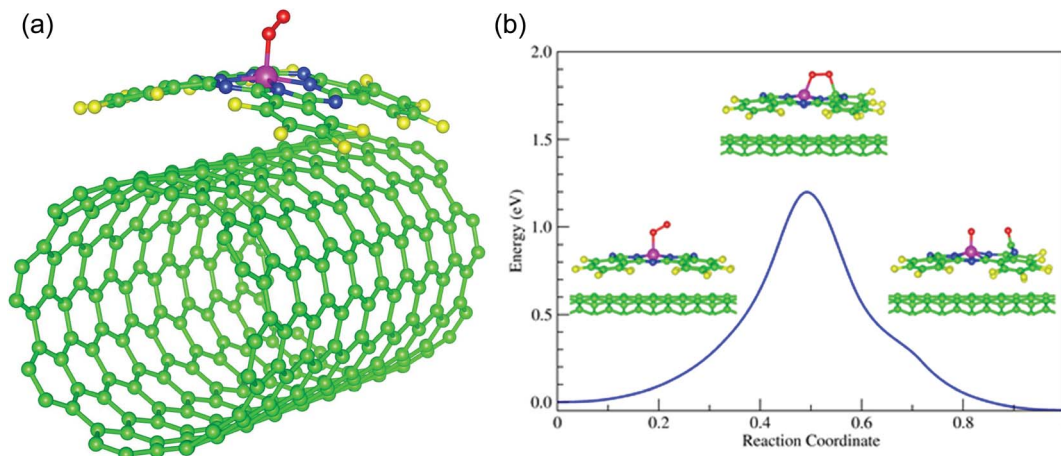


Fig. 4 (a) Equilibrium geometry for O_2 adsorbed on the metal center of the 16(F)FePc-CNT, complex in the end-on configuration. (b) Minimum energy path for the O_2 dissociation after its adsorption on the metal center of the 16(F)FePc-CNT complex. Calculations performed with the NEB method.

the Fe metal centre. The most stable s state has two unpaired electrons (magnetic moment $m = 2 \mu_B$). The states with moment $m = 0$ and $m = 4 \mu_B$ are also rather stable but with a much higher energy of 0.232 and 0.197 eV, respectively (results in Table 2). In Fig. 4(a) is shown the equilibrium geometry of the O_2 molecule adsorbed on the metal centre of the 16(F)FePc-CNT complex. The 16(F)FePc molecule firmly sticks to the CNT external walls through π -stacking or van der Waals interactions. The binding energy of 16(F)FePc on the CNT is quite strong (2.078 eV, Table 3) and comparable to covalent bonds. The most stable structure of the complex has a magnetic moment of $m = 2 \mu_B$. Other allowed spin states are $m = 0$ and $m = 4 \mu_B$ with binding energies of 2.116 and 2.518 eV, respectively. Because of the strong π -stacking interaction between 16(F)FePc and the CNT, the 16(F)FePc molecule follows the CNT curvature with a distance from the CNT surface of 3.36 Å. O_2 is adsorbed on the Fe metal centre with an end-on configuration, with O_2 tilted to the plane of the 16(F)FePc molecule, as shown in Fig. 4. The possibility that O_2 binds to the metal centre by a side-on configuration (with O–O parallel to the plane of the 16(F)FePc molecule) was also considered. However, this geometry was shown to be unstable and relaxed to the end-on one. The end-on orientation promotes the splitting of the O–O bond involving a lower energy transition state and therefore lower activation energy for the process. From simulation after O–O bond

breakage one O atom would be stabilized by a hydrogen bond to one of the C atoms before the release of a hydroxyl anion. The most stable state of the 16(F)FePc-CNT adduct has a magnetic moment of $m = 0$, which means that the spin of the metal centre couples antiferromagnetically with the spin of the O_2 molecule. The adduct is also stable with the $m = 2 \mu_B$ and $m = 4 \mu_B$ spin states with 0.042 and 0.196 eV higher in energy, respectively.

The results for O_2 binding to the metallic centre of the (16F)FePc-CNT are shown in Table 3. In the most stable spin state, $m = 0$, the binding energy of O_2 is 0.655 eV and its bond length of 1.322 Å, which is 6.4% longer than that of in the O_2 gas-phase. For the other allowed spin states, the O_2 binding energy decreases, confirming that the $m = 0$ state is the most stable spin coupling of the adduct. An energy barrier of 1.2 eV for the dissociation energy of O_2 when adsorbed on the metal centre was calculated through the NEB method, as was the minimum energy path (Fig. 4(b)). In the saddle point, the O_2 molecule binds with both Fe and C atoms, showing that the dissociation occurs on the surface of the 16(F)FePc-CNT catalyst. The energy barrier for O_2 dissociation on a Pt(111) surface has been calculated to be of 0.7 eV.⁴³ The ORR energy barrier obtained by 16(F)FePc-CNT, of 1.2 eV, suggests a good performance comparable to Pt. The binding energy for the FeN4 and the CoN4 complexes in the presence of CNT was calculated and reported in Table 4. Activities for the same complexes for the

Table 3 Theoretical results for the binding energy of the 16(F)FePc molecule adsorbed on a (8,8) CNT, for the allowed spin states (m). Total energy (E_{total}) of 16(F)FePc-F-CNT complex, also with an adsorbed O_2 molecule (O_2 -16(F)FePc-CNT) for the allowed spin states. E_0 is the lowest energy state. Binding energy (E_b) of O_2 adsorbed on the metallic center of the 16(F)FePc-CNT complex for the allowed spin states. $d_{FePc-F-CNT}$, d_{Fe-N4} , d_{O-O} , and d_{Fe-O} are bond distance between respective atoms

m (μ_B)	16(F)FePc-CNT				O_2 -16(F)FePc-CNT				
	E_b 16(F)FePc (eV)	$d_{FePc-F-CNT}$ (Å)	d_{Fe-N4} (Å)	E_{total} (eV)	E_{total} (eV)	E_b (O_2) (eV)	d_{O-O} (Å)	d_{Fe-O} (Å)	
0	−2.116	3.358	1.947	$E_0 + 0.232$	E_0	−0.655	1.322	1.832	
2	−2.078	3.359	1.954	E_0	$E_0 + 0.042$	−0.612	1.322	1.890	
4	−2.518	3.359	1.955	$E_0 + 0.197$	$E_0 + 0.196$	−0.458	1.315	2.064	

Table 4 Theoretical results for the magnetic moment (m) and O₂ binding energy (E_{bind}), for FePc-CNT, 16(Cl(FePc))-CNT, CoPc-CNT, 16(F)CoPc-CNT and 8 β (2-Et-C₆H₁₁O)CoPc-CNT in their lowest energy state

Compound	m (μ_{B})	O ₂ E_{bind} (eV)
16(F)FePc-CNT	0	-0.655
FePc-CNT	0	-0.730
16(Cl)FePc-CNT	0	-0.660
16(F)CoPc	1	-0.325
CoPc	1	-0.380
8 β (2-Et-C ₆ H ₁₁ O)CoPc	1	-0.345

ORR were extracted from previous publications.^{17,44} The values are reported in the graphical abstract where the activity of the complexes at -0.255 V vs. the binding energy are correlated. From these values a volcano correlation is reported in the graphical abstract. The calculated binding energy of O₂ to Fe and the measured electrocatalytic activity of the complex agree with positioning this complex on the top of a volcano correlation where binding energy and activities are reported for several MN4 complexes.

4. Conclusions

Fe hexadecafluorophthalocyanine (16(F)FePc) was studied as an electrocatalyst for the ORR. Because of fluorine substituents on the phthalocyanine ligand, electrons are dislocated from the Fe center. EPR and XPS spectroscopy confirmed the pulling effect of F⁻ atoms. After exposition of the catalyst to O₂ a significant energy shift of 1.5 eV was observed during XPS experiments, indicating the presence of a stable Fe-O₂ adduct. 16(F)FePc-CNT exhibited the most positive redox potential for the Fe(III)/Fe(II) couple and the highest activity towards the ORR among previously studied MN4. DFT calculations for the O₂-M binding energy and the minimum energy path for the O₂ dissociation were performed for various MN4. If the electrocatalytic activities of the MN4 at constant driving force of the electrode versus the M-O₂ binding energy of each particular catalyst were compared a volcano-shaped curve was obtained. 16(F)FePc-CNT sits at the top of this volcano and is the most active MN4 catalyst for the ORR.

Conflicts of interest

The authors state that there are no conflicts to declare.

Acknowledgements

F. T. thanks for financial support the Fondecyt Project 1181840, and Proyecto Basale Dicyt. J. H. Z. thanks the financial support of Millennium Project RC120001, Project Anillo ACT 1412 and Dicyt-USACH, Fondecyt 1140199. W. O. thanks financial support from Fondecyt Project 1170480 and the Powered@NLHPC supercomputing infrastructure of the NLHPC (ECM-02). C. A. thanks CONICYT grant FB0807. The authors

acknowledge the laboratory of free radicals for use of the EPR (USACH) and CONICYT-FONDEQUIPEQM140060. G. A. thanks FONDECYT-Iniciación No. 11170879. The authors thank Dr Ingrid Ponce for fruitful advices on the experimental procedures for the XPS experiments and the LNLS-CNPEM (Brazil) for the project 20170843 (SXS beam-line).

References

- J. H. Zagal, S. Griveau, J. F. Silva, T. Nyokong and F. Bedioui, *Coord. Chem. Rev.*, 2010, **254**, 2755–2791.
- A. B. Sorokin, *Chem. Rev.*, 2013, **113**, 8152–8191.
- H. Lu and N. Kobayashi, *Chem. Rev.*, 2016, **116**, 6184–6261.
- R. Jasinski, *Nature*, 1964, **201**, 1212–1213.
- T. Sun, B. Tian, J. Lu and C. Su, *J. Mater. Chem. A*, 2017, **5**, 18933–18950.
- J. Yang, F. Toshimitsu, Z. Yang, T. Fujigaya and N. Nakashima, *J. Mater. Chem. A*, 2017, **5**, 1184–1191.
- J. Yang, J. Tao, T. Isomura, H. Yanagi, I. Moriguchi and N. Nakashima, *Carbon*, 2019, **145**, 565–571.
- K. Kumar, P. Gairola, M. Lions, N. Ranjbar-Sahraie, M. Mermoux, L. Dubau, A. Zitolo, F. Jaouen and F. Maillard, *ACS Catal.*, 2018, **8**, 11264–11276.
- N. Ramaswamy, U. Tylus, Q. Jia and S. Mukerjee, *J. Am. Chem. Soc.*, 2013, **135**, 15443–15449.
- J. H. Zagal, I. Ponce, D. Baez, R. Venegas, J. Pavez, M. Paez and M. Gulppi, *Electrochem. Solid-State Lett.*, 2012, **15**, B90–B92.
- J. H. Zagal, F. Javier Recio, C. A. Gutierrez, C. Zuñiga, M. A. Páez and C. A. Caro, *Electrochem. Commun.*, 2014, **41**, 24–26.
- A. A. Gewirth, J. A. Varnell and A. M. DiAscro, *Chem. Rev.*, 2018, **118**, 2313–2339.
- X. Huang and J. T. Groves, *Chem. Rev.*, 2018, **118**, 2491–2553.
- N. Zion, A. Friedman, N. Levy and L. Elbaz, *Adv. Mater.*, 2018, **30**, 1800406.
- M. J. Workman, A. Serov, L.-k. Tsui, P. Atanassov and K. Artyushkova, *ACS Energy Lett.*, 2017, **2**, 1489–1493.
- J. H. Zagal and M. T. M. Koper, *Angew. Chem., Int. Ed.*, 2016, **55**, 14510–14521.
- R. Venegas, F. J. Recio, C. Zuniga, M. Viera, M.-P. Oyarzun, N. Silva, K. Neira, J. F. Marco, J. H. Zagal and F. Tasca, *Phys. Chem. Chem. Phys.*, 2017, **19**, 20441–20450.
- C. Linares-Flores, J. Espinoza-Vergara, J. H. Zagal and R. Arratia-Perez, *Chem. Phys. Lett.*, 2014, **614**, 176–180.
- J. Masa, K. Ozoemena, W. Schuhmann and J. H. Zagal, *J. Porphyrins Phthalocyanines*, 2012, **16**, 761–784.
- M. Busch, N. B. Halck, U. I. Kramm, S. Siahrostami, P. Krttil and J. Rossmeisl, *Nano Energy*, 2016, **29**, 126–135.
- M. T. M. Koper, *J. Electroanal. Chem.*, 2011, **660**, 254–260.
- A. Morozan, S. Campidelli, A. Filoramo, B. Joussetme and S. Palacin, *Carbon*, 2011, **49**, 4839–4847.
- F. Tasca, W. Harreither, R. Ludwig, J. J. Gooding and L. Gorton, *Anal. Chem.*, 2011, **83**, 3042–3049.
- A. Pizarro, G. Abarca, C. Gutierrez-Ceron, D. Cortes-Arriagada, F. Bernardi, C. Berrios, J. F. Silva,

- M. C. Rezende, J. H. Zagal, R. Onate and I. Ponce, *ACS Catal.*, 2018, **8**, 8406–8419.
- 25 S. B. P. Giannozzi, N. Bonini, M. Calandra, R. Car, C. Cavazzoni, D. Ceresoli, G. L. Chiarotti, M. Cococcioni, I. Dabo, A. Dal Corso, S. de Gironcoli, S. Fabris, G. Fratesi, R. Gebauer, U. Gerstmann, C. Gougoussis, A. Kokalj, M. Lazzeri, L. Martin-Samos, N. Marzari, F. Mauri, R. Mazzarello, S. Paolini, A. Pasquarello, L. Paulatto, C. Sbraccia, S. Scandolo, G. Sclauzero, A. P. Seitsonen, A. Smogunov, P. Umari and R. M. Wentzcovitch, *J. Phys.: Condens. Matter*, 2009, **21**, 395502.
- 26 K. Lee, É. D. Murray, L. Kong, B. I. Lundqvist and D. C. Langreth, *Phys. Rev. B: Condens. Matter Mater. Phys.*, 2010, **82**, 081101.
- 27 K. F. Garrity, J. W. Bennett, K. M. Rabe and D. Vanderbilt, *Comput. Mater. Sci.*, 2014, **81**, 446–452.
- 28 B. L. U. G. Henkelman and H. A. Jonsson, *J. Chem. Phys.*, 2000, **113**, 9901–9904.
- 29 J. G. Jones and M. V. Twigg, *Inorg. Chem.*, 1969, **8**, 2018–2019.
- 30 A. A. Tanaka, C. Fierro, D. A. Scherson and E. Yeager, *Mater. Chem. Phys.*, 1989, **22**, 431–456.
- 31 J. Zagal, M. Páez, A. A. Tanaka, J. R. dos Santos and C. A. Linkous, *J. Electroanal. Chem.*, 1992, **339**, 13–30.
- 32 R. Venegas, F. J. Recio, J. Riquelme, K. Neira, J. F. Marco, I. Ponce, J. H. Zagal and F. Tasca, *J. Mater. Chem. A*, 2017, **5**, 12054–12059.
- 33 J. Zagal, P. Bindra and E. Yeager, *J. Electrochem. Soc.*, 1980, **127**, 1506–1517.
- 34 H. Fujii, T. Yoshimura and H. Kamada, *Inorg. Chem.*, 1996, **35**, 2373–2377.
- 35 A. MacCragh, C. B. Storm and W. S. Koski, *J. Am. Chem. Soc.*, 1965, **87**, 1470–1476.
- 36 V. S. Vasani and R. J. Cross, *J. Chem. Phys.*, 1982, **77**, 4507–4514.
- 37 M. C. Biesinger, B. P. Payne, A. P. Grosvenor, L. W. M. Lau, A. R. Gerson and R. S. C. Smart, *Appl. Surf. Sci.*, 2011, **257**, 2717–2730.
- 38 R. W. Bigelow, K. Y. Law, D. H. K. Pan and H. J. Freund, *J. Electron Spectrosc. Relat. Phenom.*, 1988, **46**, 1–17.
- 39 J. Conradie and E. Erasmus, *Polyhedron*, 2016, **119**, 142–150.
- 40 E. Erasmus, *J. Electron Spectrosc. Relat. Phenom.*, 2018, **223**, 84–88.
- 41 R. Cao, R. Thapa, H. Kim, X. Xu, M. Gyu Kim, Q. Li, N. Park, M. Liu and J. Cho, *Nat. Commun.*, 2013, **4**, 2076–2082.
- 42 A. B. P. Lever, *Inorg. Chem.*, 1990, **29**, 1271–1285.
- 43 W. Orellana, *J. Phys. Chem. C*, 2013, **117**, 9812–9818.
- 44 J. Riquelme, K. Neira, J. F. Marco, P. Hermosilla-Ibáñez, W. Orellana, J. H. Zagal and F. Tasca, *Electrochim. Acta*, 2018, **265**, 547–555.